Available online at www.sciencedirect.com
SCIENCE DIRECT®
Journal of Catalysis 225 (2004) 86–94
JOURNAL OF CATALYSIS
www.elsevier.com/locate/jcat

The adhesion and shape of nanosized Au particles in a Au/TiO_2 catalyst

N. Lopez,[a,b,*] J.K. Nørskov,[b] T.V.W. Janssens,[c] A. Carlsson,[c] A. Puig-Molina,[c] B.S. Clausen,[c] and J.-D. Grunwaldt [c,1]

[a] *Departament de Quimica Fisica, Universitat de Barcelona, Marti i Franques 1, 08028 Barcelona, Spain*
[b] *Center for Atomic-scale Materials Physics, CAMP, Department of Physics, Technical University of Denmark, DK-2800 Lyngby, Denmark*
[c] *Haldor Topsøe A/S, Nymøllevej 55, DK-2800 Lyngby, Denmark*

Received 12 January 2004; revised 18 March 2004; accepted 26 March 2004
Available online 24 April 2004

Abstract

The adhesion, shape, and electronic structure of gold particles supported on $TiO_2(110)$ have been determined by density-functional theory calculations, to gain more insight into the catalytic activity of small supported gold particles. These calculations show that gold particles do not bind to a perfect TiO_2 surface, but have a binding energy of about 1.6 eV/defect on an oxygen vacancy in TiO_2. This results in an indirect effect of the support material on the catalytic activity: The distribution and dynamics of the oxygen vacancies determine the dispersion and shape of the gold particles, which in turn affect the catalytic activity. A theoretical analysis of the gold particle shape reveals that it is flat, about 3–4 layers for a gold particle of 3 nm diameter. The calculated flat geometry is in good agreement with electron microscopy and EXAFS measurements of a high surface area Au/TiO_2 catalyst containing 2.4 wt% gold.

1. Introduction

In recent years, the catalytic properties of finely dispersed gold particles on oxidic support materials have attracted much attention. Such catalysts are active for several types of oxidation reactions, in particular low-temperature CO oxidation. The selective oxidation of CO in the presence of hydrogen, a key reaction in the purification of reformate gases, is a possible application of gold-based catalysts, to which considerable research efforts have been devoted in the past few years [1–5].

Bulk gold itself is an inert material [6], and the reason why small gold particles have a catalytic activity is still a matter of debate [2,7–17]. At present we know that the catalytic activity of gold catalysts critically depends on the support material, the preparation method, and the activation procedure [2,8–10,12,13]. The explanations for the catalytic activity proposed so far have mainly focused on the size of the gold particles and the nature of the metal oxide support [2,8–13,16].

To explain the observed differences in activity with different support materials, it has been proposed that oxidic gold sites, or gold-support interface sites, are responsible for the activity in CO oxidation [18–21]. With this background, Schubert et al. [16] proposed that the metal oxide support serves as oxygen supplier, and they distinguish active support materials, which can supply oxygen to the Au particles, e.g., TiO_2, Fe_2O_3, and inert support materials, which cannot, e.g., Al_2O_3. Although such an effect may contribute to the activity of gold catalysts, the fact that Au on the inert $MgAl_2O_4$ and Al_2O_3 support has a catalytic activity as well [22–24] indicates that this is not an adequate explanation. A third explanation, which combines the effects of particle size and support material, is that the support material induces strain in the Au particles due to the mismatch of the lattices at the interface [25], an effect that is more pronounced in small gold particles than in larger ones.

A more fundamental approach to explain the catalytic activity of gold is to determine how the active gold atoms in small particles differ from bulk gold, which does not have a measurable catalytic activity. Density-functional calculations on Au clusters show that oxygen and carbon monoxide can adsorb on gold atoms with a coordination number less than 8 [26]. In fact, since the Au–Au coordination number affects the reactivity of the Au to a much larger extent than

* Corresponding author.
E-mail address: n.lopez@qf.ub.es (N. Lopez).
[1] Present address: Institute of Chemical and Bioengineering, ETH Hönggerberg, CH-8093 Zürich, Switzerland.

0021-9517/$ – see front matter © 2004 Published by Elsevier Inc.
doi:10.1016/j.jcat.2004.03.036

effects related to the electronic structure, support or strain, the coordination number can be considered to be on the top of a hierarchy of contributions that determines the catalytic activity of gold. The presence of low coordinated Au atoms is therefore a key factor for the catalytic activity of Au nanoparticles [27]. The CO oxidation involves adsorption of these molecules, and the presence of low-coordinated gold atoms is therefore a feasible explanation for the catalytic activity of gold for CO oxidation. The requirement for low-coordinated sites for CO adsorption has been corroborated by infrared spectroscopy for CO adsorption on Au/TiO_2, Au/ZrO_2, and Au/FeO catalyst systems [11,28]. Edge and corner atoms in the gold particles have a coordination number lower than 8, and therefore these atoms constitute the active sites in the gold catalysts. Note that a low-coordinated Au atom is not necessarily the only prerequisite for high catalytic activity, as there may be other conditions that need to be fulfilled as well. The concave site for CO oxidation on Au/MgO, proposed by Molina and Hammer, is an example [29]. However, high-coordinated Au atoms with catalytic activity can be excluded.

The need of low-coordinated gold atoms explains both an enhanced activity for small gold particles and the effect of the support material on the catalytic activity. Since the relative amount of edge and corner atoms increases with decreasing particle size, small gold particles are beneficial for the catalytic activity [27]. The same argument also leads to the conclusion that the shape of the gold particles is an important factor as well, as the relative amount of corner and edge atoms is larger in flat particles than in round particles with the same diameter [11]. Because the shape of a gold particle depends on the interaction between the gold and the support, different support materials induce gold particle shapes with a varying amount of edge and corner atoms. Another catalytic system showing a pronounced effect of the particle shape on the activity is the Cu/ZnO system used for methanol synthesis. A combined in situ EXAFS and in situ transmission electron microscopy (TEM) study demonstrates that the Cu particles become flat when exposed to synthesis gas (a mixture of CO, CO_2, and H_2) at reaction temperature (approximately 250 °C), possibly due to the increased amount of defects at the ZnO surface [30,31].

To gain more insight into the shape of small Au particles, we present density-functional theory (DFT) calculations for Au on TiO_2. The shape of the small gold particles is determined in two steps. First, the interaction energy of the Au on the TiO_2 surface is calculated. Then, a Wulff construction is applied to determine the shape of the gold particles. Finally, the results are compared with scanning transmission electron microscopy (STEM), EXAFS, and CO-oxidation activity measurements on a high surface area Au/TiO_2 catalyst.

2. Methods

2.1. Theoretical approach

To calculate the interaction between a gold particle and the TiO_2 support material using DFT, the TiO_2 is modeled by periodic slabs with the rutile (110) surface exposed to vacuum—the most stable phase and crystal plane of TiO_2. The slabs consist of three layers of the O–Ti_2O_2–O unit and four times the interlayer space for the vacuum with a total thickness of 19.56 Å. The supercell configuration applied in the calculations is a (1×2) $TiO_2(110)$. The interaction with Au is calculated by adding a monolayer of gold to one of the sides of the TiO_2 slabs, while correcting for the electrostatic interaction between the cells and the adsorbate-induced polarization [32]. Relaxation is allowed only for the two outermost surface layers and the adsorbed gold atoms. In that way a complete interaction between a (111)-like Au deposit and the $TiO_2(110)$ surface is achieved, in agreement with the experimentally determined contact plane between Au and $TiO_2(110)$ [33]. Fig. 1 displays a drawing of the slab models used in the calculations for Au on TiO_2.

To evaluate the electronic structure after adsorption of the Au atoms, ultrasoft pseudopotentials are used to describe the ionic cores [34]. The exchange–correlation energy is described by the generalized gradient approximation PW91 [35]. The Kohn–Sham one-electron valence states are expanded in a basis of plane waves with kinetic energies below 340 eV, and the surface Brillouin zone is sampled by a Monkhorst–Pack mesh of $[4 \times 1 \times 1]$. Fermi population of the Kohn–Sham states ($k_B T = 0.2$ eV) and Pulay mixing of

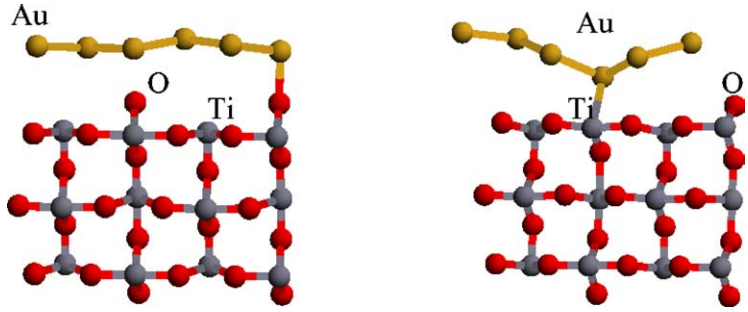

Fig. 1. Ball and stick models for the interaction of a monolayer of gold with a perfect rutile $TiO_2(110)$ surface (left), and with oxygen defects in the rutile $TiO_2(110)$ surface (right).

the resulting electronic density [36] have been applied. The total energies have been extrapolated to $k_B T = 0$ eV, and the final energies have been calculated through the RPBE functional [37].

The shape of gold particles on the TiO_2 surface is determined by means of a Wulff construction. According to this construction, the shape of a particle is found by truncating a crystal in all directions at distances proportional to the surface free energy of the crystal plane in that direction. To apply a Wulff construction for a supported particle, one has to know what crystal plane is directed toward the support, and the corresponding interface energy [38,39], since the interaction with the support modifies the surface energy of that contact plane. As noted above, the Au(111) plane is in contact with the rutile (110) surface [33]. The interface energy, however, is difficult to obtain experimentally, but it is readily available from DFT calculations.

To derive the shape of the supported gold particle, we use the ratio between the contact surface free energy of the supported gold particle (γ) and the surface free energy of the gold particle without interaction (γ_0). The energy balance for adsorption results in the following expression for this ratio,

$$\frac{\gamma}{\gamma_0} = \frac{(\gamma_{\text{int}} - \gamma_{\text{ox}})}{\gamma_0} = 1 + \frac{\Delta E}{A\gamma_0}, \tag{1}$$

where γ_{int} is the interface energy, γ_{ox} is the surface energy of the oxide support, ΔE is the total binding energy at the metal-oxide interface, and A is the contact area. From this equation, it is easily deduced that this parameter is equal to 1 if there is no interaction between the gold and the TiO_2 surface, and becomes less than 1 if there is an interaction ($\Delta E < 0$) between the gold particle and the support. Fig. 2 shows the shape of a small gold particle for several values of γ/γ_0, using the Wulff construction. Clearly, the particles become flat when the interaction increases.

The Wulff construction is only an approximation, because it does not account for the formation energies for edge and corner atoms. For small particles the contribution of edges and corners becomes significant. Therefore, another model to calculate the height of the particles is presented, which accounts for edges and corners by using the energy values for these low-coordinated atoms calculated by DFT.

2.2. Experimental

The catalyst used for the activity measurements, the STEM, and EXAFS experiments was prepared by precipitation of Au colloids on TiO_2, and contained 2.4 wt% Au. The measured activity of this catalyst for CO oxidation at 50 °C is 2.3 ± 0.15 $\text{mmol}_{\text{CO}}\,\text{mol}_{\text{Au}}^{-1}\,\text{s}^{-1}$ after heat treatment to 400 or 500 °C, using a feed of 1% CO, 21% O_2, and 78% Ar.

The STEM experiments were performed on a Philips CM200 electron microscope operated at 200 kV, with a probe size of approximately 0.3 nm. To obtain a high contrast for the gold particles, a high angle annular dark-field

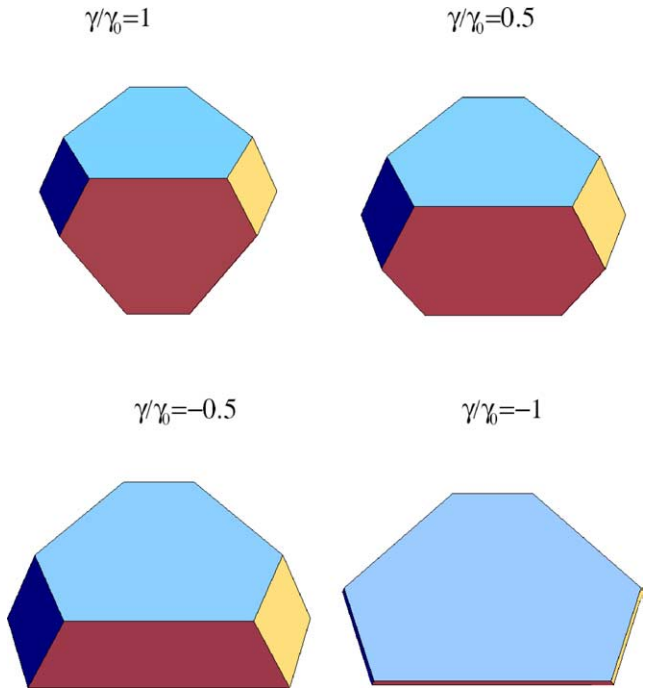

Fig. 2. Geometries for gold on a rutile TiO_2(110) surface, derived from a Wulff construction, for different values of the interface energy (γ/γ_0). The top right structure is the best representation for the shape of gold particles on a TiO_2 support.

(HAADF) detector was used. For each sample 10–15 images were recorded at a magnification of 500,000, corresponding to an image resolution of 0.154 nm/pixel. In the STEM experiments, we used a sample of the catalyst that had been treated in exactly the same way as in the activity measurements, in a separate reactor system.

The EXAFS measurements were performed at beamline X1 of the HASYLAB synchrotron at the AuL_3 edge in transmission mode, using a double Si(111) crystal monochromator. A reactor cell with full control of gas atmosphere and temperature was used. The catalyst in the reactor cell was heated for 1 h to several temperatures in the range 200–600 °C in an atmosphere 1% CO, 21% O_2, and 78% Ar, and cooled to 25 °C after each treatment to measure the EXAFS spectra. The Au–Au coordination numbers (N) were corrected for inharmonic effects, using $N_{\text{corr}} = N_{\text{measured}} + 36T\alpha(12 - N_{\text{measured}})$ [40], where T is the temperature in the EXAFS experiment, and α is the linear expansion coefficient for gold ($14.2 \times 10^{-6}\ \text{K}^{-1}$).

3. Results

The interaction between gold and a TiO_2 surface is evaluated for two possible structures of gold on TiO_2, shown in Fig. 1. The model to the left corresponds to adhesion of a monolayer of gold on a perfect rutile TiO_2(110] surface, and the model to the right to a monolayer of gold adsorbed on an oxygen vacancy in the TiO_2 surface with a missing-row structure. This is a well-known reconstruction of the

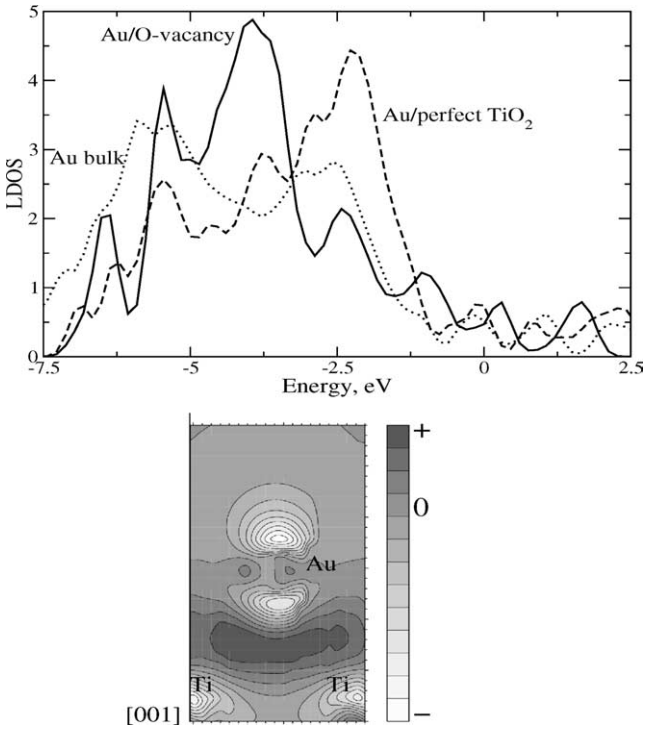

Fig. 3. (Top) Density of states (DOS) for different Au structures: bulk gold, an adsorbed monolayer of gold on rutile TiO_2(110) surface, and the gold atom in a monolayer attached to an oxygen defect in the rutile TiO_2(110) surface. The interaction between gold and an oxygen vacancy in the TiO_2 surface causes a shift in the DOS to higher binding energies. (Bottom) Electron density difference plot for a gold atom on an oxygen vacancy in the rutile TiO_2 with respect to Au and oxygen vacancy in TiO_2 before interaction. A charge accumulation is seen between Au and the Ti atoms close to the vacancy.

TiO_2 surface, in which a complete row of protruding oxygen is removed, thus providing a large amount of oxygen vacancy defects. The oxygen vacancy density in this structure is 2.56 nm^{-2}.

The most important result from the calculations is that the interaction between a monolayer of gold, representative of a large gold particle, and a perfect rutile TiO_2(110] surface (Fig. 1, left) is negligibly small [41], while the interaction on a TiO_2 surface with oxygen vacancies (Fig. 1, right) yields an interaction energy of -1.6 eV/defect, which corresponds to -0.5 J/m^2. This means that oxygen vacancy sites, and possibly other surface defect sites, such as step or adatom sites, are required to bind the gold to a TiO_2 surface. A similar result has been found for the binding of single Au atoms and small Au clusters on TiO_2 [42,43]. A scanning tunneling microscopy study of Au particles on a rutile TiO_2(110) surface confirms this conclusion [44]. The effect of the support in the Au/TiO_2 system is indirect: The support provides the defects necessary for Au adhesion, and a change in the vacancy density affects the dispersion and shape of the Au particles, and therefore presumably also the catalytic properties.

Fig. 3 shows the local density of states for bulk gold, a monolayer of Au on a perfect TiO_2 surface, and a Au atom

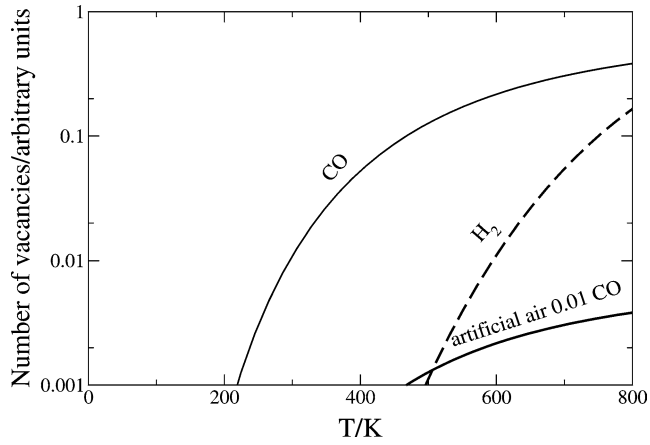

Fig. 4. Estimated number of vacancies in the surface of rutile TiO_2(110) for different ambient gas atmospheres.

on an oxygen vacancy. The gold atoms adsorbed on a perfect rutile TiO_2(110) have no significant charge, and their electronic structure around the Fermi level is almost unperturbed, consistent with the very weak interaction at the interface. For adhesion on an oxygen vacancy, the bands corresponding to the gold atoms in direct contact with the vacancy are stabilized, but these perturbations are confined to the nearest neighbors only, because the electronic screening is very effective [45,46]. In fact, the density-difference plot shows that the electrons are accumulated between the gold and the two titanium atoms next to the vacancy (see Fig. 4), and that the bond is covalent, resembling that of an alloy. Since the perturbation of the electronic structure is local, it is expected that the crystal faces of supported gold particles largely behave as unsupported gold, and are therefore not able to bind CO or O_2 stronger than corresponding crystal faces in gold, even at the atoms directly in contact with the vacancy on TiO_2.

Because gold adhesion exclusively occurs on the defects in TiO_2, anything that affects these defects in the TiO_2 surface, e.g., a reaction that produces or consumes oxygen vacancies in the TiO_2, will probably affect the catalytic properties of a Au/TiO_2 catalyst. Reactions with reducing compounds such as H_2 or CO may produce oxygen vacancies, while in oxidizing atmospheres, oxygen vacancies may be consumed. Such reactions probably occur in the commonly applied heat treatments to activate the Au/TiO_2 catalysts, and they determine the final size and shape of the gold particles in the activated catalyst.

To illustrate the effects of the gas atmosphere on the defect density in TiO_2, the number of defects as a function of the temperature in an atmosphere of H_2, CO, and diluted CO is estimated. To do this, we have estimated the equilibrium constants, using formation energies of the oxygen vacancies, and H_2 and H_2O or CO and CO_2. Due to the stoichiometry of the reaction, the number of defects is equal to the equilibrium amounts of H_2O or CO_2, which are calculated from the equilibrium constants. Fig. 4 shows the estimated amounts of defects produced as a function of temperature in the pres-

ence of H_2 and CO for a 2×2 reconstruction of the TiO_2 surface. These data show that both H_2 and CO produce more vacancies at higher temperatures, and that the amount of vacancies depends on the type and amount of the gases present.

To derive the shape of the gold particles, the ratio γ/γ_0, [Eq. (1)]—or the interface energy—is the key parameter. The interaction between the gold and the TiO_2 surface [ΔE in Eq. (1)], however, depends on the number of oxygen vacancies below the gold particle. For a particle with a diameter of 3 nm the adhesion energy E_d of -1.6 eV/defect calculated above, and a γ_0 equal to 0.3 eV/atom (3.85 eV/nm^2), the ratio γ/γ_0 becomes 0.76 for 4 defects and 0.53 for 8 defects. The approximate shape of the gold particles found by a Wulff construction therefore corresponds to the top right one in Fig. 2, which has $\gamma/\gamma_0 = 0.5$.

Information about the shape of the gold particles can also be obtained by estimating how the gold particles grow on a TiO_2 surface. To do this, we have calculated the number of atoms in the gold particle, at which transitions from single-layered to double-layered and multilayered particles occur. The number of atoms at which these transitions occur depends on the interface energy, which results from the number of defects underneath a gold particle. From the number of particles at the transitions and the number of layers, a particle diameter can be estimated. On the basis of these data a shape diagram as displayed in Fig. 5 can be constructed, showing the number of layers for a given number of defects (interface energy) and particle diameter.

To perform this analysis, the following assumptions have been made: The particles used in the model consist of a given number of atoms (N), equally distributed over a number of layers (L). Each layer is assumed to have a circular geometry, which implies that there are no corner atoms in this model. To simplify the model, we assume that all bonding of Au to TiO_2 occurs at an oxygen vacancy; the interface energy is then directly proportional to the number of oxygen vacancies in the Au/TiO_2 interface; adhesion at other defect sites can easily be incorporated by adjusting the number of oxygen vacancies in the model. We also include the energies for the edges, as they may contribute significantly to the total energy in small particles. Then, the energy of the particles is given by the equations below.

For a single-layer particle,

$$E_{\text{particle}}^{1\text{ML}} = \gamma_0^{1\text{ML}} N + n_d E_d^{1\text{ML}} + 2\pi\sqrt{N} E_{\text{edge}}^{1\text{ML}}; \tag{2}$$

for a multilayer particle,

$$E_{\text{particle}}^{L\text{ML}} = \gamma_0^{L\text{ML}} \frac{2N}{L} + n_d E_d^{L\text{ML}} + 4\pi\sqrt{\frac{N}{L}} E_{\text{edge,top-bottom}}^{L\text{ML}} + 2(L-2)\pi\sqrt{\frac{N}{L}} E_{\text{edge,central}}^{L\text{ML}}, \tag{3}$$

where N is the number of atoms in a particle, L is the number of layers in a particle. $\gamma_0^{L\text{ML}}$ is the surface energy for a particle with L layers, n_d is the number of defects underneath the particle, E_d is the defect energy, $E_{\text{edge,top-bottom}}$ is the energy of the edge atoms in the top and bottom layer, $E_{\text{edge,central}}$ is the edge energy for the central layers in the particles.

The energy values to be used in these equations are listed in Table 1, and are estimated from calculations of slabs containing 1 to 4 gold layers. The values for the edges have been found by comparing the energies of a L layer slab and a small aggregate with the same number of layers. The shape diagram calculated on the basis of the energy values listed in Table 1 is displayed in Fig. 5. According to these calculations, a Au particle with a diameter of 3–4 nm, a typical

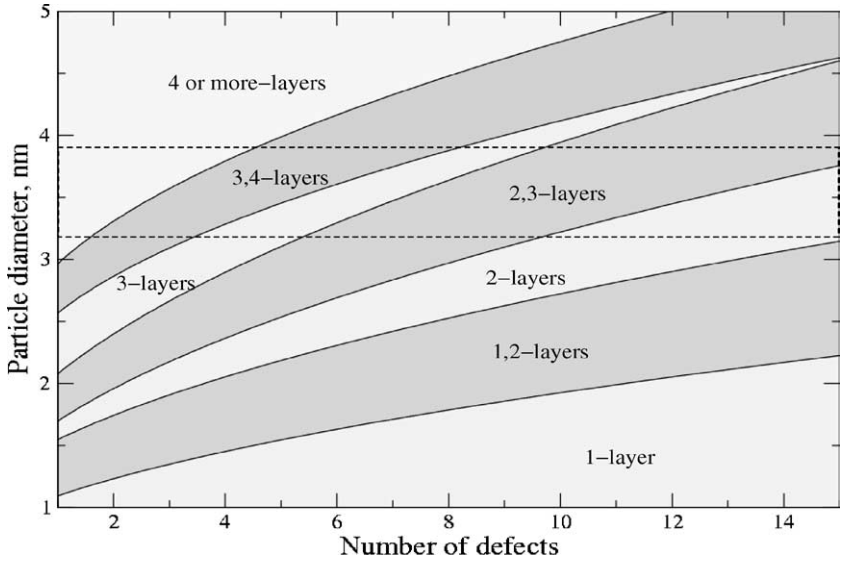

Fig. 5. Shape diagram for Au supported on TiO_2(110). The diagram represents the particle diameter as a function the interface energy, given by the number of defects below the particle, using the energy values in Table 1. The different regions indicate where n-layered structures are stable. The region inside the dotted square corresponds to the experimentally determined average particle diameter. The dashed line indicates an estimated maximum concentration for defects under the one-layer particle.

Table 1
Calculated energy values for surface energy, defect energy, and edge energies, as applied in the determination of the gold particle shape

Thickness	1 layer	2 layers	3 layers
Surface energy (γ_0, eV/atom)	0.60	0.29	0.26
Defect energy (E_d, eV/defect)	−1.6	−0.2	2.3
Edge energy top–bottom ($E_{edge,top-bottom}$, eV/atom)	0.25	0.33	0.33
Edge energy center ($E_{edge,center}$, eV/atom)			0.41

particle size for Au in Au/TiO_2 catalysts, is 3 to 4 layers thick, which corresponds to approximately 0.75–1 nm. This means that the gold particles are flat, in good agreement the thickness of Au particles on flat supports [47–50].

The presence of flat particles in a real Au/TiO_2 catalyst, as found in the theoretical model, is addressed by combining the results of STEM and EXAFS measurements on a high surface area Au/TiO_2 catalyst. Fig. 6 displays representative STEM images of a Au/TiO_2 catalyst after 1 h of heating in a mixture of 1% CO, 21% O_2, 78% Ar at 400 °C (left) and 500 °C (right). In the bottom panel, the particle size distributions determined from these image series, based on approximately 1500 particles, are given. The average diameter of the Au particles in this Au/TiO_2 catalyst is 3.4 nm after heating to 400 °C and 3.8 nm after heating to 500 °C.

Fig. 7 shows the Au–Au coordination number derived from EXAFS as a function of the heating temperature in the pretreatment. Heating the Au/TiO_2 catalyst results in a higher Au–Au coordination number, indicating a sintering of the Au particles. The Au–Au coordination number in the Au/TiO_2 catalyst after the heat treatment at 400 and 500 °C is 10.6. For "spherical" particles ($\gamma/\gamma_0 = 1.0$) with the measured size distribution, the coordination number would be 11.3; for a "hemispherical" particle this would be 11.1. For flat particles with the diameters of the measured size distribution, and a thickness of about 3–4 layers of Au in the range

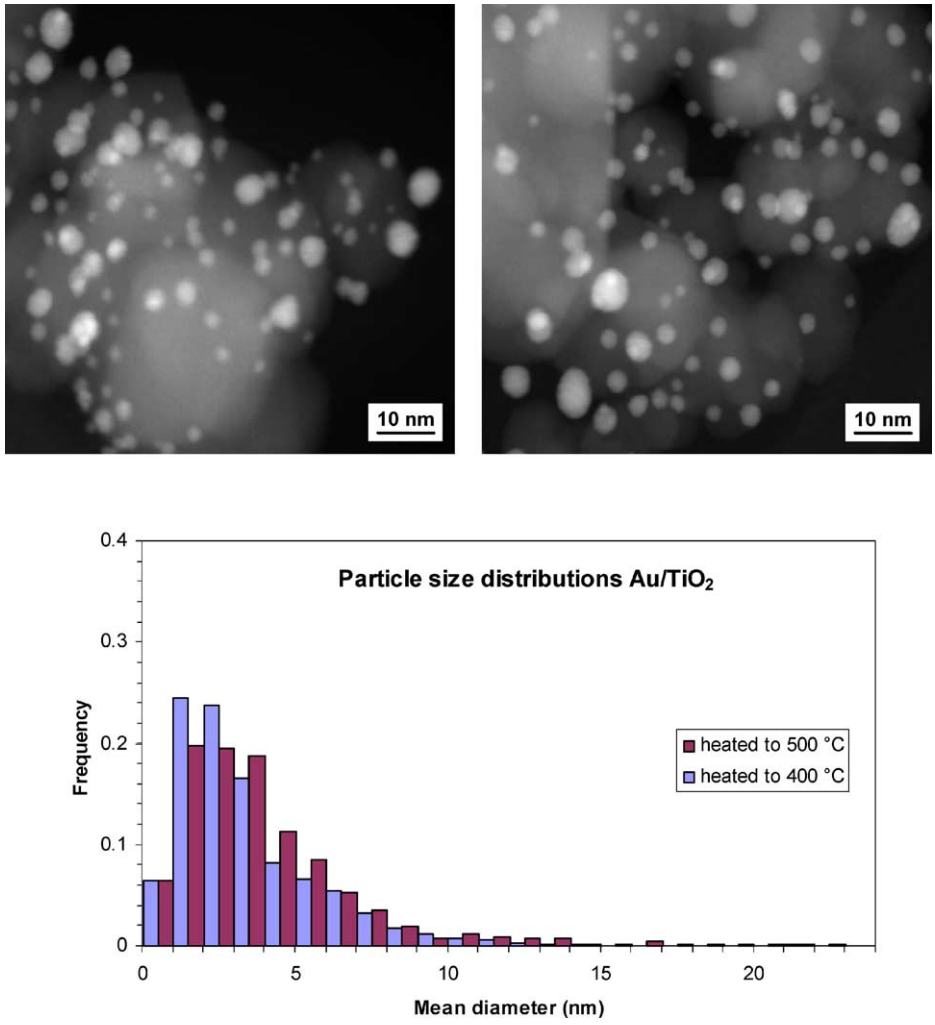

Fig. 6. (Top) Scanning transmission electron microscopy (STEM) images of a Au/TiO_2 catalyst (2.4 wt% Au) after 1 h of heating in 1% CO, 21% O_2, 78% Ar at 400 °C (left) and 500 °C (right). (Bottom) Particle size distributions derived from the STEM image series measured after these treatments.

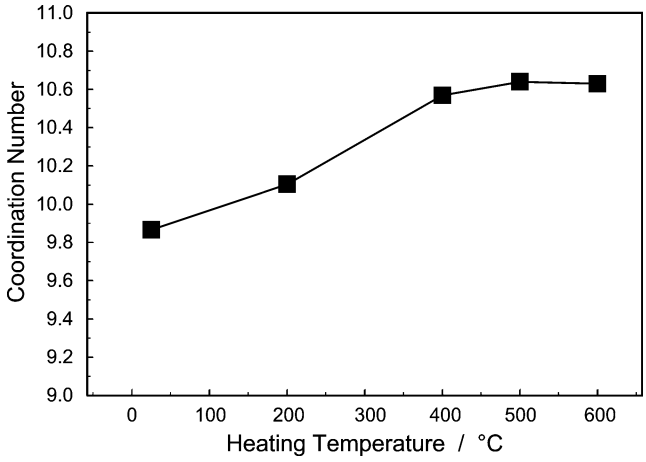

Fig. 7. Corrected Au–Au coordination number determined by EXAFS for a Au/TiO_2 catalyst (2.4 wt% Au) after 1 h of heating in 1% CO, 21% O_2, 78% Ar at several temperatures.

2–4 nm as predicted in the model, the estimated coordination number is 10.7. This experimental result indicates that the geometry of the gold particles as found from the model is a realistic option for the Au particle shape in high surface area Au/TiO_2 catalysts.

The Au–Au distances derived from the EXAFS experiments were all 2.87 ± 0.02 Å, which corresponds nicely to the Au–Au distance in bulk gold (2.88 Å). This indicates that there is no significant contraction or expansion of the crystal lattice in the gold particles in the catalyst, which is inconsistent with the proposal that catalytic activity of small gold particles is caused by tension in the gold lattice.

4. Discussion

The results of our calculations show that the adhesion of gold to the TiO_2 does not occur on a perfect TiO_2 surface, but requires oxygen defects, or possibly steps or adatoms. Since TiO_2 is a reducible oxide, oxygen vacancies are commonly present in TiO_2 [51,52]. Even a clean rutile-TiO_2(110) surface contains 5–10% surface oxygen defects [44,52,53]; the TiO_2 material used for preparing the supported catalysts probably has even more. The preference for adhesion of the gold particles on oxygen vacancies is experimentally confirmed by scanning tunneling microscopy (STM), in which a large reduction of the amount of oxygen vacancies in the surface has been detected after metal deposition [44]

The interaction between the gold and the support determines both the size and the shape of the gold particles, as can be derived from the data in Fig. 5. As low-coordinated Au atoms are necessary for adsorption of O or CO [26], and the amount of low-coordinated Au atoms depends both on the size and on the shape of the particle, the catalytic activity is also expected to depend on the size and shape of the Au particles. In particle size distributions, no information about the particle shape is included. Therefore, a different particle shape can explain why Au particles of the same size can have a different activity on different supports [11,54,55].

Wahlström et al. explain how the diffusion of oxygen vacancies and gold particles on a TiO_2 surface proceeds, based on STM observations [44]. The oxygen vacancies themselves diffuse on the surface in the presence of oxygen in the gas phase [56]. The gold particles, not sufficiently attached to oxygen vacancies, diffuse on the surface, and they grow when they coalesce with another gold particle (sintering), or diffusion slows down or stops when they encounter other oxygen vacancies, due to the increased interface energy. This finally leads to a stable situation, where the gold particles have accumulated so many vacancies that diffusion stops. This accumulation of vacancies under the gold particles implies a higher interface energy, and therefore, there is a tendency for the formation of flat gold particles in the Au/TiO_2 system (Fig. 5).

Water reacts with the oxygen vacancies on a TiO_2 surface [53], and will therefore affect the interaction between the Au particles and the support. Since this effect depends on the nature of the support, this could explain why Au catalysts with different supports behave differently in the presence of traces of water. The Au/TiO_2 catalysts are very sensitive to the presence of water [9,13], while other support materials, e.g., $MgAl_2O_4$ spinel, are more robust [24]. This is an important issue, as traces of water will always be present when removing CO from the H_2 feed in fuel cells, which is a possible application for gold-based catalysts. The effect of small amounts of water on the activity of Au/TiO_2 catalysts can be rationalized as follows: Water affects the interface energy the Au and the TiO_2 support, and, consequently, both the size and the shape of the Au particles changes, similar to the effects observed in Cu/ZnO-based methanol synthesis catalysts [31]. Such a change in particle geometry leads to a change in the number of active corner and edge atoms, and therefore a change in catalytic activity.

A final and more general aspect concerns the influence of the support material on the catalytic activity of gold-based catalysts. Other support materials have a different interface energy, which results in a different gold particle shape, and therefore a different activity. The requirement of defects for adhesion of Au seems to be more general, though they are not necessarily oxygen vacancies, and is known for MgO, Al_2O_3, and SiO_2 as well [57–61]. Although the earlier suggestion that a reducible support is favorable for gold-based catalysts by supplying oxygen to the catalytic reaction may not be correct, it is easy to obtain oxygen vacancies on reducible supports. Therefore, such materials are expected to be good supports, as there are many sites available for adhesion of gold particles.

Other aspects of catalysis with gold-based catalysts, such as effect of exposure to certain gases, or the influence of the support seem to be rationalized by analysis of the effect of defects on the interface energy between the gold particles and the support. With defects acting as anchoring sites for

the gold particles, the behavior of these defects under different conditions affects the behavior of the catalyst. Therefore, a good knowledge of the support material is essential for understanding catalysis by gold.

5. Conclusions

Density-functional calculations for gold on a rutile-TiO_2 (110) surface show that the adhesion energy of gold particles on a perfect TiO_2 surface is negligibly small and defects are required to obtain stable gold particles. Very common defects on a TiO_2 surface are oxygen vacancies, and they can be regarded as anchoring sites for the gold particles, together with other defects like steps and adatoms.

The effect of the support material on the catalytic activity of Au/TiO_2 catalysts is indirect, with the interface energy as key parameter. The final size and shape of the gold particles is determined by the interface energy between the Au particles and the TiO_2 surface. Oxygen vacancies contribute to this interface energy, and therefore determine the size and shape of the gold particles, and with that the number of active sites. Based on a model calculation with the interface energy as parameter, it is deduced that the gold particles in a Au/TiO_2 catalyst are flat typically 3–4 layers for particles with a diameter of 3 nm. This conclusion is supported by a combined microscopy and EXAFS characterization of the gold particles in a high-surface Au/TiO_2 catalyst.

Acknowledgments

Financial support from the Danish National Research Foundation through the Center for Atomic-Scale Materials Physics (CAMP), and from SNF through Dansync, and beamtime at HASYLAB are gratefully acknowledged. N. Lopez thanks EU for Grant HPMF-CT-2000-00431, financial support through the Ramon y Cajal program of the Spanish Ministry of Science and Technology and the Catalan government through the BE-2003 program.

References

[1] R.J.H. Grisel, B.E. Nieuwenhuys, J. Catal. 199 (2001) 48.
[2] M. Haruta, Catal. Today 36 (1997) 153.
[3] J.A. Rodriguez, G. Liu, T. Jirsak, J. Hrbek, Z. Chang, J. Dvorak, A. Maiti, J. Am. Chem. Soc. 124 (2002) 5242.
[4] R.M.T. Sanchez, A. Ueda, K. Tanaka, M. Haruta, J. Catal. 168 (1997) 125.
[5] M.M. Schubert, V. Plzak, J. Garche, R.J. Behm, Catal. Lett. 76 (2001) 143.
[6] B. Hammer, J.K. Nørskov, Nature 376 (1995) 238.
[7] M.A. Bollinger, M.A. Vannice, Appl. Catal. B 8 (1996) 417.
[8] G.C. Bond, D.T. Thomson, Catal. Rev.-Sci. Eng. 41 (1999) 319.
[9] J.-D. Grunwaldt, C. Kiener, C. Wögerbauer, A.J. Baiker, J. Catal. 181 (1999) 223.
[10] J.-D. Grunwaldt, A. Baiker, J. Phys. Chem. B 103 (1999) 1002.
[11] J.-D. Grunwaldt, M. Maciejewski, O.S. Becker, P. Fabrizioli, A. Baiker, J. Catal. 186 (1999) 458.
[12] M. Haruta, in: 3rd World Congress on Oxidation Catalysis, San Diego, 1997, p. 123.
[13] M. Haruta, M. Daté, Appl. Catal. A 222 (2001) 427.
[14] U. Heiz, A. Sanchez, S. Abbet, W.-D. Schneider, Eur. Phys. J. 9 (1999) 35.
[15] A. Sanchez, S. Abbet, U. Heiz, W.-D. Schneider, H. Hakkinen, R.N. Barnett, U. Landman, J. Phys. Chem. A 103 (1999) 9573.
[16] M.M. Schubert, S. Hackenberg, A.C. van Veen, M. Muhler, V. Plzak, R.J. Behm, J. Catal. 113 (2001) 197.
[17] M. Valden, X. Lai, D.W. Goodman, Science 281 (1998) 1647.
[18] G.R. Baumweda, S. Tsubota, T. Nakamura, M. Haruta, Catal. Lett. 44 (1997) 83.
[19] F. Boccuzzi, A. Chiorino, S. Tsubota, M. Haruta, J. Phys. Chem. B 100 (1996) 3625.
[20] S. Minico, S. Scire, C. Crisafulli, A.M. Visco, S. Galvagno, Catal. Lett. 47 (1997) 273.
[21] S. Tsubota, T. Nakamura, K. Tanaka, M. Haruta, Catal. Lett. 56 (1998) 131.
[22] M. Okamura, S. Nakamura, S. Tsubota, T. Azuma, M. Haruta, Catal. Lett. 51 (1998) 53.
[23] S.-J. Lee, A. Gravriilidis, J. Catal. 206 (2002) 305.
[24] J.-D. Grunwaldt, H. Teunissen, Eur. patent EP1209121 (2002).
[25] M. Mavrikakis, P. Stoltze, J.K. Nørskov, Catal. Lett. 64 (2000) 101.
[26] N. Lopez, J.K. Nørskov, J. Am. Chem. Soc. 124 (2002) 11262.
[27] N. Lopez, T.V.W. Janssens, B.S. Clausen, Y. Xu, M. Mavrikakis, T. Bligaard, J.K. Nørskov, J. Catal. 223 (2004) 232.
[28] C. Lemire, R. Meyer, S. Shaikhutdinov, H.-J. Freund, Angew. Chem. Int. Ed. 43 (2004) 118.
[29] L.M. Molina, B. Hammer, Phys. Rev. Lett. 90 (2003) 206102.
[30] J.-D. Grunwaldt, A.M. Molenbroek, N.-Y. Topsøe, H. Topsøe, B.S. Clausen, J. Catal. 194 (2000) 452.
[31] P.L. Hansen, J.B. Wagner, S. Helveg, J.R. Rostrup-Nielsen, B.S. Clausen, H. Topsøe, Science 295 (2002) 2053.
[32] J. Neugebauer, M. Scheffler, Phys. Rev. B 46 (1992) 16067.
[33] F. Cosandey, T.E. Madey, Surf. Rev. Lett. 8 (2001) 73.
[34] D.H. Vanderbilt, Phys. Rev. B 41 (1990) 7892.
[35] J.P. Perdew, et al., Phys. Rev. B 46 (1992) 6671.
[36] G. Kresse, J. Forthmüller, Comput. Mater. Sci. 6 (1996) 15.
[37] B. Hammer, L.B. Hansen, J.K. Nørskov, Phys. Rev. B 59 (1999) 7413.
[38] B.S. Clausen, J. Schiøtz, L. Gråbæk, C.V. Ovesen, K.W. Jacobsen, J.K. Nørskov, H. Topsøe, Top. Catal. 1 (1994) 367.
[39] T. Worren, K.H. Hansen, E. Lægsgaard, F. Besenbacher, I. Stensgaard, Surf. Sci. 477 (2001) 8.
[40] B.S. Clausen, J.K. Nørskov, Top. Catal. 10 (2000) 221.
[41] N. Lopez, J.K. Nørskov, Surf. Sci. 515 (2002) 175.
[42] Y. Wang, G.S. Hwang, Surf. Sci. 542 (2003) 72.
[43] A. Vittadini, A. Selloni, J. Chem. Phys. 117 (2002) 353.
[44] E. Wahlström, N. Lopez, R. Schaub, P. Thostrup, C. Afich, E. Lægsgaard, J.K. Nørskov, F. Besenbacher, Phys. Rev. Lett. 90 (2003) 026101.
[45] L. Giordano, J. Goniakowski, G. Pacchioni, Phys. Rev. B 64 (2001) 075417.
[46] B. Hammer, Phys. Rev. Lett. 89 (2002) 016102.
[47] V.A. Bondzie, S.C. Parker, C.T. Campbell, Catal. Lett. 63 (1999) 143.
[48] S.C. Parker, A.W. Grant, V.A. Bondzie, C.T. Campbell, Surf. Sci. 441 (1999) 10.
[49] C. Lemire, R. Meyer, S. Shaikhutdinov, H.-J. Freund, Surf. Sci. 552 (2004) 27.
[50] Sh.K. Shaikhutdinov, R. Meyer, M. Naschitzki, M. Bäumer, H.J. Freund, Catal. Lett. 86 (2003) 211.
[51] U. Diebold, J.F. Anderson, K.-O. Ng, D. Vanderbilt, Phys. Rev. Lett. 77 (1996) 1322.

[52] M. Li, W. Hebenstreit, U. Diebold, M. Tyrsyshkin, M.K. Bowman, G.G. Dunham, M.A. Henderson, J. Phys. Chem. B 104 (2000) 4944.
[53] R. Schaub, P. Thostrup, N. Lopez, E. Lægsgaard, I. Stensgaard, F. Besenbacher, Phys. Rev. Lett. 87 (2001) 266104.
[54] M. Haruta, S. Tsubota, T. Kobayashi, H. Kageyama, M.J. Genet, B. Delmon, J. Catal. 144 (1993) 175.
[55] E.D. Park, J.S. Lee, J. Catal. 186 (1999) 1.
[56] R. Schaub, E. Wahlström, A. Rønnau, E. Lægsgaard, I. Stensgaard, F. Besenbacher, Science 299 (2003) 377.
[57] U. Diebold, Surf. Sci. Rep. 48 (2003) 53.
[58] A.M. Ferrari, G. Pacchioni, J. Phys. Chem. 100 (1996) 9032.
[59] Z. Lodziana, J.K. Nørskov, J. Chem. Phys. 115 (2001) 11621.
[60] Z. Lodziana, J.K. Nørskov, Surf. Sci. 518 (2002) L577.
[61] N. Lopez, F. Illas, G. Pacchioni, J. Am. Chem. Soc. 121 (1998) 913.